applied sciences

MDPI

Article

Prediction Equation for Horizontal Ground Motion Peak Values in the Loess Plateau Region

Wei Wan [1,2,*], Jingshan Bo [1] and Da Peng [1]

[1] Institute of Disaster Prevention, Yanjiao 065201, China; bojingshan@163.com (J.B.); pengda@cidp.edu.cn (D.P.)
[2] Hebei Key Laboratory of Earthquake Disaster Prevention and Risk Assessment, Sanhe 065201, China
* Correspondence: wanwei@cidp.edu.com; Tel.: +86-188-3161-2212

Abstract: This study collects all strong motion records from 134 seismic events in the Loess Plateau region of China between 2020 and 2023. The corresponding ground motion attenuation dataset is constructed through data processing and screening, including 1149 soil horizontal strong ground motion records. Based on this dataset, two ground motion attenuation models are developed. Specifically, through magnitude grouping and weighted processing, two-step fitting methods are used to establish prediction equations for the peak ground acceleration (PGA), effective peak acceleration (EPA), and peak ground velocity (PGV) at the horizontal soil layers. These equations can estimate ground motion parameters with magnitudes ranging from M_S 3.0 to M_S 6.5 and epicentral distances between 0 and 100 km. Furthermore, attenuation curves are plotted based on the prediction equations. A comparison between the actual observed values and the predicted curves and an evaluation of the fitting residuals assess our models' fitting performance. The attenuation characteristics of horizontal ground motion parameters in the Loess Plateau region are systematically summarized.

Keywords: Loess Plateau of China; ground motion attenuation; strong motion records; attenuation model; peak ground acceleration (PGA); effective peak acceleration (EPA); peak ground velocity (PGV)



Academic Editor: Dario De Domenico

Received: 24 November 2024
Revised: 15 January 2025
Accepted: 16 January 2025
Published: 22 January 2025

Citation: Wan, W.; Bo, J.; Peng, D. Prediction Equation for Horizontal Ground Motion Peak Values in the Loess Plateau Region. *Appl. Sci.* **2025**, *15*, 1098. https://doi.org/10.3390/app15031098

Copyright: © 2025 by the authors. Licensee MDPI, Basel, Switzerland. This article is an open access article distributed under the terms and conditions of the Creative Commons Attribution (CC BY) license (https://creativecommons.org/licenses/by/4.0/).

1. Introduction

Destructive seismic events have frequently occurred in the Loess Plateau region of China, causing significant casualties and property damage [1]. The loess, widely distributed across the region, has unique soil dynamics characteristics, leading to notable regional variations in seismic activity and damage distribution. Therefore, studying the ground motion attenuation behavior in this specific soil layer can significantly improve earthquake disaster prevention and mitigation efforts. With the continuous improvement of China's National Strong Motion Observation Network, many strong motion records have been recently accumulated from the Loess Plateau region, providing reliable data for establishing prediction equations for ground motion parameters applicable to this area. Building upon existing research, this study uses the latest strong motion records to develop prediction equations for horizontal ground motion parameters in the Loess Plateau region.

The study of ground motion attenuation relationships requires a substantial amount of strong motion records. With advancements in observation technology and the widespread deployment of instruments, the global collection of strong motion records has significantly increased. This progress has provided robust support for research on ground motion attenuation relationships [2].

In the early stages, the lack of sufficient strong motion records in the Loess Plateau region made it impossible to directly establish ground motion parameter prediction equations through statistical methods. Instead, the prediction of peak ground motion in this region relied on the conversion method proposed by Hu. This method established attenuation relationships for peak ground motion on bedrock [3,4], which were then used to predict ground motion parameters at engineering sites.

Research on attenuation relationships of peak ground motion parameters for the Loess Plateau began in the 1980s. Ding et al. divided historical seismic intensity data into loess and bedrock regions [5]. By comparing data from the western United States, they derived bedrock ground motion attenuation relationships using the intensity-distance method. They suggested adjusting loess ground motion parameters to bedrock values by a factor of 0.6 or amplifying bedrock parameters by a factor of 1.67 to reflect soil amplification effects.

Some researchers used administrative boundaries to conduct regional studies based on seismic intensity maps. For instance, Wen analyzed seismic intensity data from the Shanxi seismic belt and established intensity attenuation relationships for the region [6]. Zhou et al. performed regression analysis on intensity data from 20 earthquakes of magnitude 5 or higher in Gansu Province, deriving attenuation relationships specific to the province [7]. Fan et al. established separate intensity attenuation relationships for the northern Loess Plateau, the southern Qinba Mountains, and the Guanzhong Plain in Shaanxi Province. Using data from the western United States, they applied a mapping conversion method to derive bedrock attenuation relationships for these regions [8].

Yang and Luo analyzed 1221 strong motion records collected from soil sites in the loess regions of Shaanxi, Gansu, Qinghai, and Ningxia during the Wenchuan earthquake. Using direct fitting methods, they derived horizontal and vertical peak acceleration attenuation relationships for the Loess Plateau [9]. Subsequently, other researchers [10–12] conducted extensive studies in the Loess Plateau and other loess regions to address engineering demands or specific research needs.

Existing studies show that ground motion attenuation in loess-covered areas is slower than in nearby non-loess areas. This difference becomes more pronounced for larger earthquakes and aligns with observed macro-seismic damage patterns.

This study collects 4010 strong motion records from 134 seismic events in the Loess Plateau region, which are analyzed and screened, ultimately constructing the dataset required for the prediction equations. Each strong motion record is processed with baseline correction and high-pass filtering and the peak parameters and epicentral distances are extracted. Subsequently, two attenuation models are developed for nonlinear data fitting, assisting the development of prediction equations for horizontal ground motion parameters at the soil layers, including peak ground acceleration (PGA), effective peak acceleration (EPA), and peak ground velocity (PGV). These equations can estimate the ground motion parameters with magnitudes ranging from M_S 3.0 to M_S 6.5 and epicentral distances between 0 and 100 km. PGA refers to the maximum absolute amplitude of the ground motion acceleration time history, measured in cm/s^2 or gal. It characterizes the intensity of the inertial effects of ground motion and reflects its high-frequency characteristics. EPA is the peak acceleration with an averaged significance based on the response spectrum. EPA is formulated as follows:

$$\mathrm{EPA} = S_a/2.5 \quad (1)$$

where S_a represents the smoothed average value of the acceleration response spectrum with a damping ratio of 5% in the frequency range of 2 to 10 Hz. *Sa* is then divided by 2.5 to obtain the EPA [13]. This study introduces the EPA parameter and analyzes its attenuation relationship to investigate further the impact of ground motion attenuation on structural damage in the Loess Plateau region.

PGV refers to the maximum absolute value of the ground motion velocity time history, measured in cm/s. It is related to the kinetic energy of particle vibrations and is a significant physical quantity for measuring ground motion energy. The velocity peak reflects the intensity of the medium-frequency components of the ground motion. Studies, such as blasting experiments, have revealed that PGV correlates well with the degree of structural damage.

Given the importance, intuitiveness, and clear physical significance of the peak parameters, PGA, EPA, and PGV, this study adopts a magnitude grouping approach. Specifically, it uses two-step fitting methods to establish the prediction equations for PGA, EPA, and PGV in the Loess Plateau region. Based on these equations, the corresponding attenuation curves and fitting residual distribution plots are generated, and the fitting performance of the two attenuation models is analyzed. Finally, based on the analysis results, a suggested selection scheme for the attenuation relationships of peak parameters in the Loess Plateau region is proposed.

2. Methods and Data

The strong motion data used in this work originate from the Strong Motion Observation Data Center of the Institute of Engineering Mechanics, China Earthquake Administration. In December 2023, the dataset was updated to include the most recent seismic event, i.e., the 6.2 magnitude earthquake on 18 December 2023, in Jishishan, Gansu.

2.1. Scope of the Strong Motion Record Dataset in the Loess Plateau Region

The study area primarily encompasses the Loess Plateau region in China, with selected seismic events located between longitudes 95 °E and 115 °E and latitudes 30 °N and 45 °N, covering seven provinces and autonomous regions, including Gansu, Shanxi, Shaanxi, Qinghai, Hebei, Inner Mongolia Autonomous Region, and the Ningxia Hui Autonomous Region.

2.2. Seismic Events in the Loess Plateau Region

This study involves 134 seismic events in the Loess Plateau region of China, including mainshocks and aftershocks. The magnitude of these events spans from M_S 2.4 to M_S 7.1, from 2001 to 2023. Figure 1 illustrates the distribution of the epicenters and stations, highlighting that the seismic events are mainly concentrated in the Qilian Mountains, Helan Mountains, and Taihang Mountains, all located within the Fenzhou, Yinchuan–Hetao, Longmenshan, and Liupan-Mountains–Qilian-Mountains seismic belts.

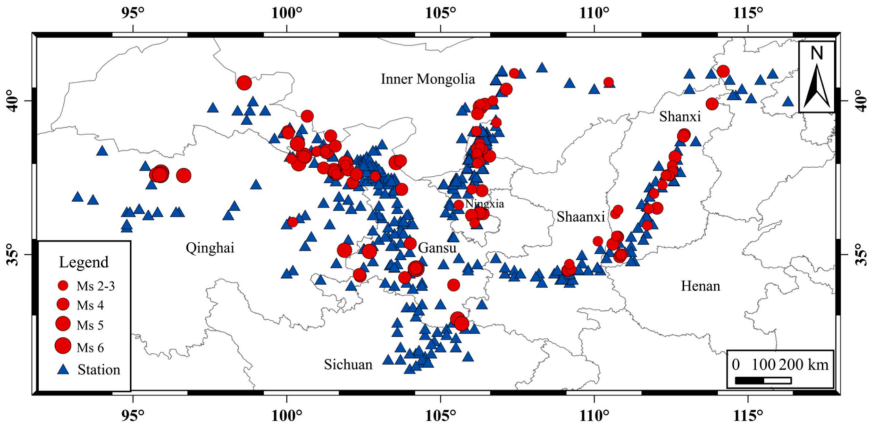


Figure 1. Distribution map of earthquakes and stations.

Table 1 reports the magnitude distribution of the seismic events, where seismic events with magnitudes between M_S 4.0 and M_S 4.9 account for the highest proportion, reaching 42.5%. The second-highest proportion involves magnitudes between M_S 3.0 and M_S 3.9, at 30.6%.

Table 1. Seismic event magnitude information.

Magnitude	Number of Seismic Events	Horizontal Strong Ground Motion Data
7	1	15
6.0–6.9	8	1268
5.0–5.9	19	888
4.0–4.9	57	1335
3.0–3.9	41	444
2.0–2.9	8	60
Total	134	4010

2.3. Distribution of Strong Motion Records in the Loess Plateau Region

A total of 4010 strong motion records are collected, including records in the east-west, north-south, and vertical directions. Among these, 2678 are horizontal and 1332 are vertical strong motion records. Table 2 lists the distribution of the strong motion records based on the epicentral distance, with distances between 30 km and 100 km accounting for 48.9% while records closer to the epicenter are relatively few. Only 99 records are within 5 km of the epicenter, accounting for approximately 2.5%.

Table 2. Spatial distribution information on strong motion records in the Loess Plateau region.

Epicentral Distance		0.0–5.0	5.1–10.0	10.1–30.0	30.0–100	100.1–200	>200	Subtotal
Magnitude	7	0	0	0	3	0	12	15
	6.0–6.9	0	12	84	807	189	176	1268
	5.0–5.9	3	12	102	345	291	135	888
	4.0–4.9	33	75	303	696	198	30	1335
	3.0–3.9	54	60	216	108	6	0	444
	2.0–2.9	9	15	33	3	0	0	60
Total		99	174	738	1962	684	353	4010

Figure 2 depicts the epicentral distance distribution of the strong motion records collected in the Loess Plateau region, revealing that the epicentral distance range broadens as the magnitude increases. Most strong motion records are concentrated within an epicentral distance of 200 km, accounting for approximately 91.2% of the total records.

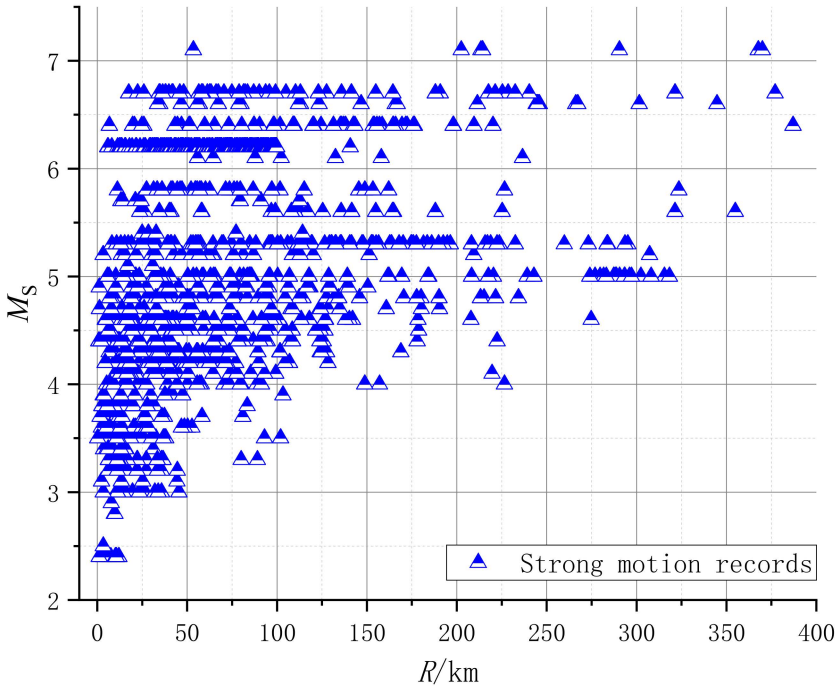


Figure 2. Magnitude-epicentral distance distribution of strong motion records in the Loess Plateau region.

2.4. Relationship Between Magnitude and the Farthest Triggering Distance of Strong Motion Instruments

Equation (2) expresses the relationship between magnitude (M_S) and the farthest triggering distance (R) of the instruments capturing strong motion in the Loess Plateau region. This parabolic relationship indicates that the farthest epicentral distance where strong motion stations are triggered increases as the magnitude increases. Notably:

$$R = -61.9 - 7.9M_S + 13.9M_S^2 \quad (2)$$

where R (unit: km) represents the farthest triggering distance and M_S (unitless) is the surface wave magnitude. This relationship is derived from strong motion observations in the Loess Plateau region. It applies to M_S values ranging from 2.4 to 7.1, with corresponding epicentral distances between 0 and 400 km.

2.5. Correlation Analysis of PGA and PGV in the Loess Plateau Region

The relationship between PGA (unit: gal) and PGV (unit: cm/s) in the Loess Plateau region is expressed as follows:

$$\mathrm{PGA} = 6.023 + 18.067 \times \mathrm{PGV} \quad (3)$$

This equation represents a statistical relationship between PGA and PGV rather than a physical conversion. Equation (3) applies to the Loess Plateau region of China for earthquakes with magnitudes (M_S) ranging from 3.0 to 6.5 and epicentral distances between 0 and 200 km.

Figure 3 depicts the distribution of PGA and PGV concerning the epicentral distance in the region while Figure 4 illustrates the fitted relationship between PGA and PGV. In Figure 4, PGV is plotted on the horizontal axis (unit: cm/s) and PGA on the vertical axis (unit: gal, equivalent to cm/s^2). The regression line in Figure 4, based on Equation (3), reveals a linear relationship between PGA and PGV, with the slope of 18.067 representing the rate at which PGA increases with PGV and the intercept of 6.023 indicating the baseline

PGA when PGV is negligible. This relationship allows straightforward estimation of one parameter from the other, providing practical insights into seismic ground motion in the Loess Plateau region.

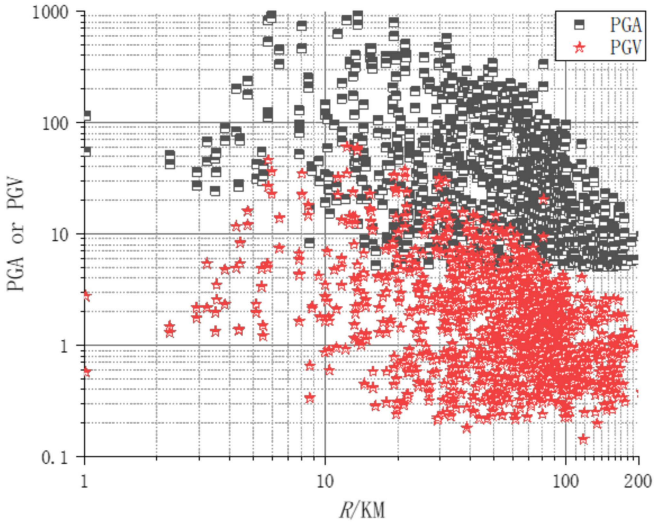


Figure 3. Distribution of PGA and PGV with respect to epicentral distance in the Loess Plateau region.

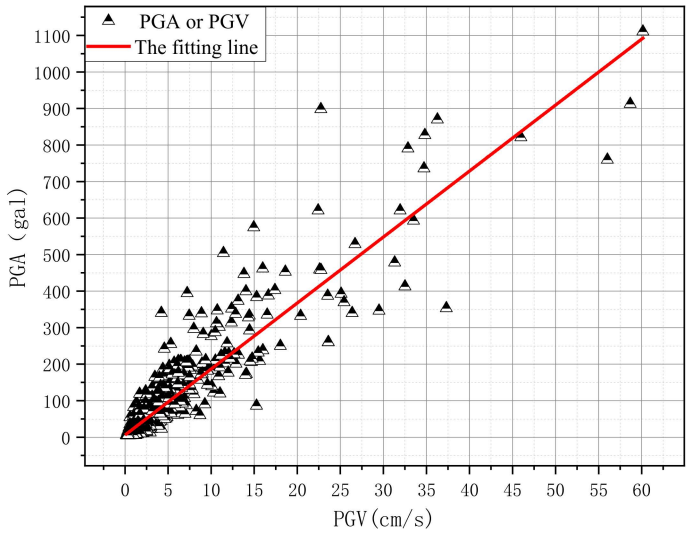


Figure 4. Fitted relationship between PGA and PGV in the Loess Plateau region.

2.6. Data Processing of Strong Motion Records

The acceleration records used are digital strong motion records with a sensor frequency response range of 0–80 Hz, a 200-sample-per-second sampling rate, and a pre-event storage capability of 10 or 20 seconds. Processing is required due to potential errors caused by the raw records' baseline drift, background noise, and sensor tilt. Low-frequency noise can cause baseline drift, which introduces significant errors when computing velocity or displacement through integration. Therefore, baseline correction must be performed before conducting the attenuation fitting analysis.

The error-handling methods include high-pass filtering to eliminate background noise, the Iwan correction method to address sensor hysteresis [14], and linear fitting to correct tilt errors in near-fault records [15]. Data processing is conducted using the relevant filtering, correction, spectral analysis, and calibration programs developed by our research team. In this study, the two horizontal component records from a single station's set of recordings are treated as two individual records, collectively called horizontal records.

2.7. Data Screening of Strong Motion Records

This study applies the following principles for screening strong motion records:

(1) Directional classification: Separate horizontal and vertical direction datasets were established. However, this study analyzes only the horizontal dataset;
(2) Amplitude screening: Due to the minimal impact of records with low PGA on engineering seismic resistance outcomes, this study excludes data where PGA is less than 5 gal to reduce the interference from low-amplitude data;
(3) Epicentral distance and station screening: This research focuses on attenuating moderate and minor earthquake strong motion records in the Loess Plateau region. Records with epicentral distances exceeding 100 km and those from non-surface stations are excluded;
(4) Site type screening: Considering the limited number and uneven distribution of data from bedrock stations, which makes it challenging to statistically derive reliable predictive models for bedrock sites, records classified under the site type "rock" are excluded;
(5) Anomalous data screening: Potential anomalous records are identified by plotting the distribution of PGA against magnitude and epicentral distance. Further waveform checks are performed using SeismoSignal software version 5.1.0 and records with obvious "spikes" or "cut-offs" are removed;
(6) Magnitude screening: These records are excluded due to the insufficient number and uneven distribution of strong motion records with magnitudes less than M_S 3.0. Additionally, records with magnitudes greater than M_S 6.7 are excluded to focus on moderate and minor earthquakes.

2.8. Attenuation Research Dataset

After screening the data based on the abovementioned steps, the dataset used to construct prediction equations for ground motion parameters of moderate and minor magnitudes in loess sites includes 1149 horizontal records. This dataset is suitable for fitting the horizontal attenuation relationships for magnitudes ranging from M_S 3.0 to M_S 6.5 and epicentral distances from 0 to 100 km. It is used to establish various prediction equations for ground motion parameters at the surface of loess soil layers.

It should be noted that the surface wave magnitude (M_S, unitless) is primarily used as the magnitude scale, owing to its wide adoption in China. Thus, most of the magnitude information in the original record headers is surface wave magnitude, with a minor portion being local magnitude (M_L, unitless). Local magnitude is converted based on the conversion formula provided in the "Earthquake Work Handbook" (China Earthquake Disaster Prevention Center, 1990) [16]:

$$M_S = 1.13M_L - 1.08 \quad (4)$$

In the attenuation relationship research, selecting the distance parameter is critical. Commonly used distance parameters include epicentral distance, hypocentral distance, fault distance, and fault projection distance, among which epicentral distance and fault distance are more widely applied. This study primarily examines the attenuation relationships of earthquakes up to a magnitude of 6.5. Since most records in the dataset do not contain information about the seismic fault, this article uses the epicentral distance (R) as the distance parameter. Epicentral distance is the horizontal distance between the station and the epicenter, which can be calculated using the geographic coordinates of the station and the epicenter.

3. Attenuation Models and Regression Algorithms

Ground motion attenuation models, or the mathematical expressions of ground motion attenuation relationships, describe the variation of ground motion with distance, source depth, and other influencing factors. Since the source mechanism influences ground motion, the propagation medium and site conditions must be included in the model.

3.1. Attenuation Models Used in This Study

This study develops two types of ground motion parameter attenuation models. Model I is the attenuation model used in the "Seismic Ground Motion Parameters Zonation Map of China" (GB18306–2015) [17], expressed as follows:

$$\lg y = \mathrm{A} + \mathrm{B}M + \mathrm{C}\lg\left(R + \mathrm{D}\mathrm{e}^{\mathrm{E}M}\right) + \xi \tag{5}$$

where EM represents the products of E and M. This notation is introduced for concise representation.

Preliminary analysis indicates a significant correlation between the attenuation rate of ground motion parameters and magnitude. To more accurately describe this relationship, this study references the related research findings [18,19] and improves the attenuation model. In the improved model, the attenuation coefficient term is a linear function of magnitude, forming Model II, proposed in this article, expressed as follows:

$$\lg y = \mathrm{A} + \mathrm{B}M + (\mathrm{F} + \mathrm{G}M)\lg\left(R + \mathrm{D}e^{\mathrm{E}M}\right) + \xi \tag{6}$$

$$\lg y = \sum_{i=1}^{m} H_i E_i + \mathrm{C}\lg\left(R + \sum_{i=1}^{m} R_{0i} E_i\right) + \varepsilon \tag{7}$$

$$R_0 = \mathrm{D}\mathrm{e}^{\mathrm{E}M} \tag{8}$$

$$H = \mathrm{A} + \mathrm{B}M \tag{9}$$

$$C = \mathrm{F} + \mathrm{G}M \tag{10}$$

Model II is introduced as part of the improved model and is described by Equation (6). Where y represents the ground motion parameter, such as PGA or PGV; M denotes the surface wave magnitude; R is the epicentral distance, measured in kilometers (km); A, B, C, D, E, F, and G are regression coefficients; and ξ is a random variable with a mean of 0 and a standard deviation of σ.

3.2. Regression Algorithms Used in This Study

After determining the functional form of the ground motion attenuation relationship, the least squares method is used to regress the seismic record data to obtain the coefficients within the model, constituting a nonlinear multivariate regression analysis problem. The data quality and the chosen regression method directly impact the results' accuracy. Indeed, the uneven distribution of observational data in magnitude, distance, seismic events, and regions mandates addressing these biases by adding weights and employing a two-step regression method. This study adopts the two-step regression method proposed by Joyner et al. in 1981 [20], which effectively decouples the correlation between magnitude and distance [21].

The first step of the two-step regression rewrites the attenuation relationship (Equation (5)) as Equation (7), where the pseudo-variable $\mathrm{E_i}$ is a binary variable, i.e., if it is the i-th earthquake, E = 1; otherwise, E = 0. At the same time, bi and $\mathrm{R_{0i}}$ represent the influence of the i-th earthquake. In the first step of regression, C is treated as a constant and the values for $\mathrm{H_i}$ and $\mathrm{R_{0i}}$ within each magnitude band are obtained using the minimum

variance principle within the estimated range of C, followed by the second regression step. The second step substitutes the values of R0i and Hi (i = 1, 2, ..., m) obtained from the first step into Equations (8) and (9) for calculation. The regression analysis provides the coefficients A, B, D, and E.

This method effectively decouples the impacts of magnitude and distance. Specifically, the first regression step does not involve magnitude and only analyzes the effect of distance, avoiding the interference of magnitude errors on the distance regression. The second regression step does not consider distance and only examines the impact of magnitude. This strategy ensures that each seismic event is given equal weight in the magnitude regression analysis, avoiding bias due to the abundance of observational data from an earthquake event.

4. Regression Analysis

This section uses the prediction equation for horizontal PGA as an example to introduce the specific process of regression analysis. Based on Model II, proposed earlier, nonlinear fitting is performed using a magnitude grouping method.

4.1. Method of Magnitude Grouping

4.1.1. Magnitude Bracketing

The significant variations in the number of samples at different magnitudes within the dataset impose high dispersion in the fitting results. Hence, after multiple trials, this study reduces the dispersion caused by magnitude using the following magnitude bracketing method (Table 3), where the average magnitude is the arithmetic mean of all magnitudes in each group.

Table 3. PGA fitting magnitude bracketing method.

Magnitude Bracket	Grouped Magnitude Data	Average Magnitude	Quantity
First Group	3.0,3.1,3.2,3.3,3.4,3.5,3.6,3.7,3.8	3.4	146
Second Group	3.9,4.0,4.1,4.2,4.3	4.2	114
Third Group	4.4,4.5,4.6,4.7	4.5	143
Fourth Group	4.8,4.9,5.0,5.1,5.2	5.0	163
Fifth Group	5.3,5.4,5.6,5.7,5.8	5.5	69
Sixth Group	6.1,6.2EW	6.2	227
Seventh Group	6.2NS,6.7,6.6,6.4	6.3	288

4.1.2. First Step of Fitting in the Magnitude Grouping Method

The average magnitude is used within the same magnitude bracket, assuming all data within the group have the same magnitude. Given a consistent magnitude, the R_0 and other magnitude-related terms in the model are treated as constants. Based on this, regression for Equation (7) is performed separately for the seven groups and the R_0 values are optimized to minimize the regression variance. Ultimately, the values of $R_{0(n)}$, $H_{(n)}$, and $C(n)$ are obtained, corresponding to each group's average magnitude (Table 4).

In the first step of fitting, R_0 is determined using a value assignment search method and the appropriate coefficients, D and E, are identified based on the equation form of R_0. The first-stage fitting results of PGA for each magnitude bracket are presented in Figures 5–8. The figures reveal that as the epicentral distance increases, the difference in PGA between higher and lower magnitudes gradually narrows and, even at distances greater than 60 km, the attenuation curve for the M_S 4.5 group is higher than that for the M_S

5.0 group. This phenomenon is primarily because each group's attenuation curve is fitted independently without imposing additional magnitude-related constraints. This makes the attenuation curves from different magnitude groups intersect at greater distances. After completing the second fitting step, the final PGA prediction equation can address this issue.

Table 4. $R_0(n)$, $H(n)$, and $C(n)$ for each magnitude bracket.

Average Magnitude (M_S)	$R_{0(n)}$	$H_{(n)}$	Standard Error of $H_{(n)}$	$C_{i(n)}$	Standard Error of $C_{i(n)}$
3.4	8	2.797	0.144	−1.037	0.115
4.15	11	3.858	0.205	−1.472	0.143
4.53	12	3.297	0.168	−1.031	0.118
5.03	15	4.364	0.224	−1.593	0.154
5.54	18	5.447	0.469	−2.089	0.296
6.2	24	6.201	0.122	−2.195	0.075
6.27	25	6.171	0.121	−2.210	0.073

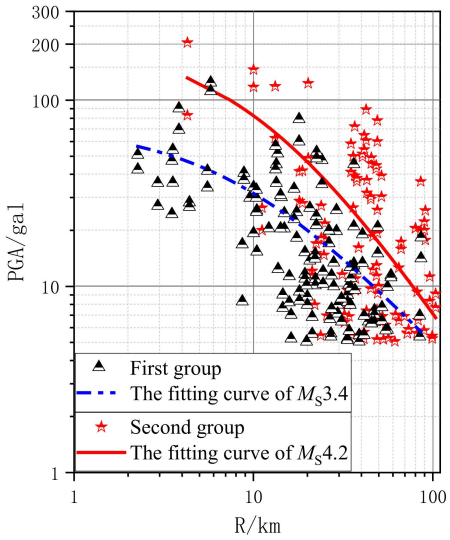


Figure 5. Attenuation curves for M_S 3.4 and M_S 4.2.

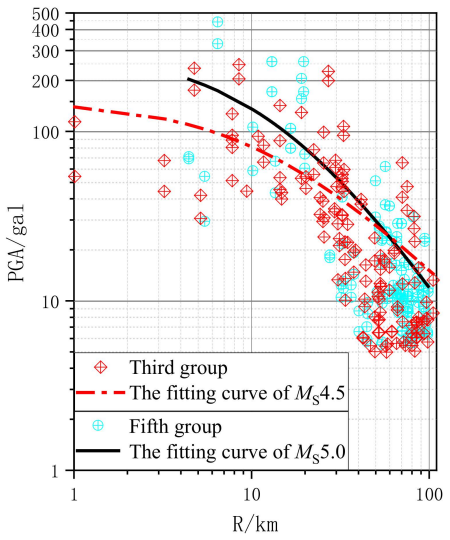


Figure 6. Attenuation curves for M_S 4.5 and M_S 5.0.

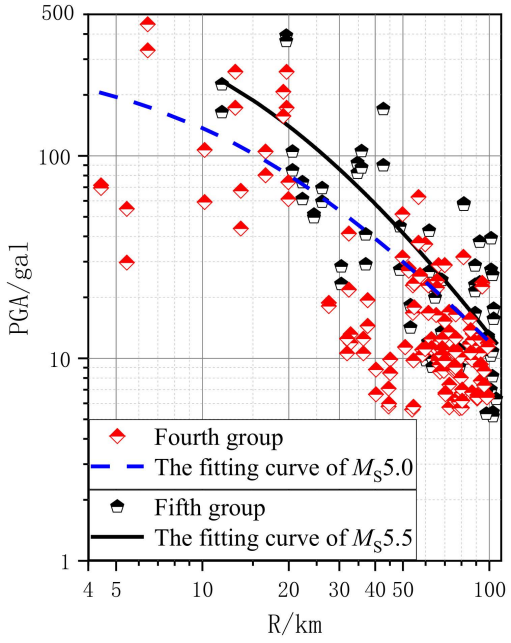


Figure 7. Attenuation curves for M_S 5.0 and M_S 5.5.

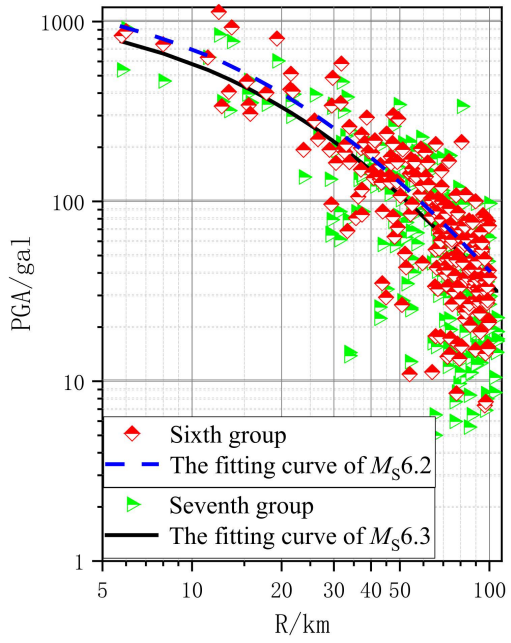


Figure 8. Attenuation curves for M_S 6.2 and M_S 6.3.

The attenuation curves in Figure 7 demonstrate a trend of gradually converging as the epicentral distance increases. Additionally, the attenuation curves in Figure 8 are nearly parallel, with the attenuation curve for the M_S 6.3 group slightly higher than that for M_S 6.2, despite the minor difference in magnitude and most of the data originating from the same earthquake.

4.1.3. Second Step of Fitting

Based on the data from Table 4, Equations (8)–(10) are used to fit R_{0i}, H_i, and C_i, respectively, with the corresponding results illustrated in Figures 9–11.

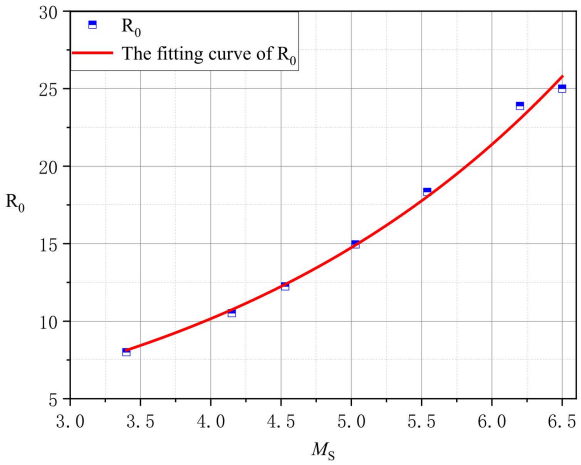


Figure 9. Fit graph for coefficient R_0.

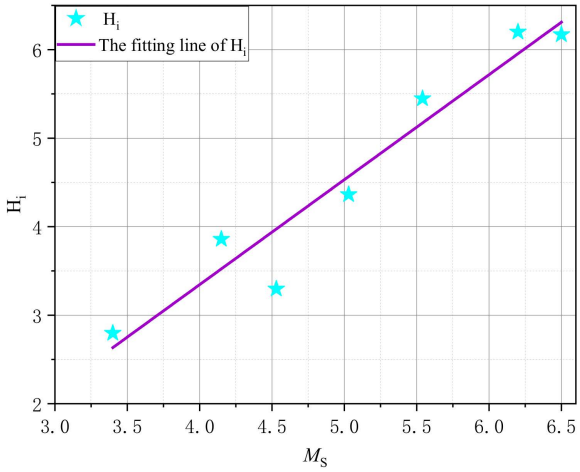


Figure 10. Fit graph for coefficient H_i.

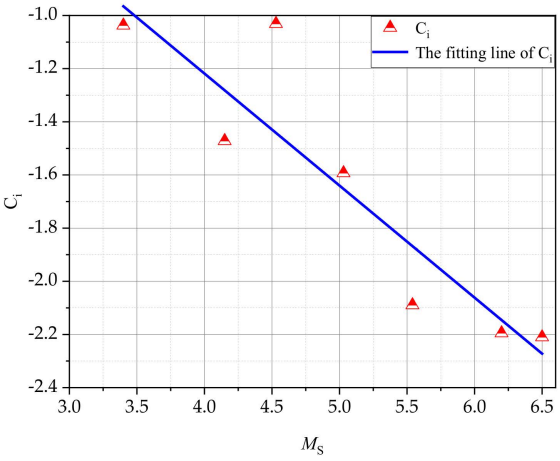


Figure 11. Fit graph for coefficient C.

When using Equation (8) for data fitting, the results indicate that D = 2.28974, rounded to three decimal places as 2.290, with a fitting standard error of 0.186, and E = 0.373, with a fitting standard error of 0.0139. The goodness of fit (adjusted R2) for this dataset is 0.993. When using Equation (9) for data fitting, the results show that A = −1.399, with a fitting standard error of 0.752, and B = 1.186, with a fitting standard error of 0.146. The goodness of fit for this dataset is 0.916. Moreover, when using Equation (10) for data fitting, F = 0.468, with a fitting standard error of 0.437, and G = −0.422, with a goodness of fit of 0.798. Compared to this, the fit of attenuation coefficient C is slightly lower than that of coefficient H.

4.1.4. Horizontal PGA Prediction Equation

The regression coefficients obtained from the fittings described above are then substituted into Model II to derive the horizontal PGA prediction equation for the Loess Plateau region, as shown in Equation (11). This equation generates the PGA prediction curves presented in Figure 12 by inserting various R and M value intervals. Figure 12 highlights that the attenuation curves for each magnitude level do not intersect and the higher the magnitude, the higher the curve. As magnitude increases, the attenuation rate accelerates, leading to a more significant difference in PGA near the epicenter than at farther distances. Additionally, Figure 12 reveals that near the epicenter (R = 1 km), the PGA predictions for M_S 6.5, 6.0, 5.0, and 3.0 earthquakes are 1164, 859, 367, 117, and 28 gal, respectively.

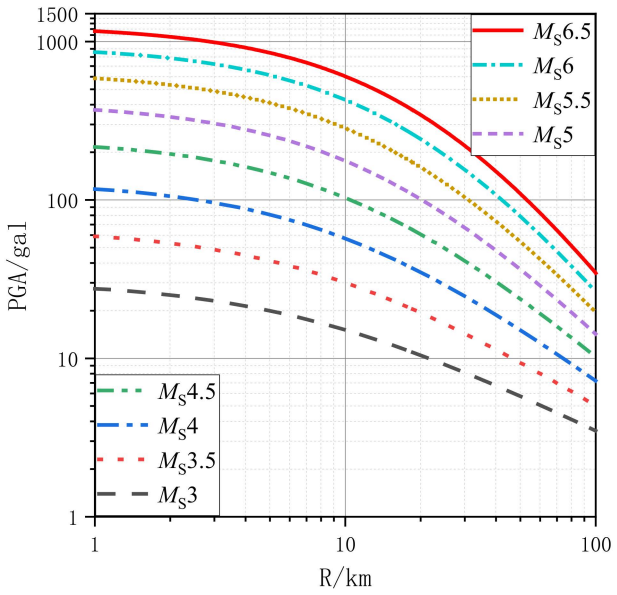


Figure 12. PGA attenuation curves fitted by the magnitude grouping method in the Loess Plateau.

Figure 13 compares the PGA attenuation curves for M_S 4.5 and M_S 5.0 earthquakes with the stepwise fitting results, suggesting that the developed PGA prediction equation aligns well with the observed values and resolves the issue of intersecting attenuation curves across different magnitudes encountered in the first step of the fitting process. Additionally, the PGA attenuation curve for a M_S 5.0 earthquake generated by Equation (11) is higher than the results from the first fitting step, primarily due to the influence of data from a M_S 6.2 earthquake, which have elevated the overall PGA prediction value for M_S 5.0.

$$\lg PGA = -1.399 + 1.186M + (0.468 - 0.422M)\lg\left(R + 2.290e^{0.373M}\right) \quad (11)$$

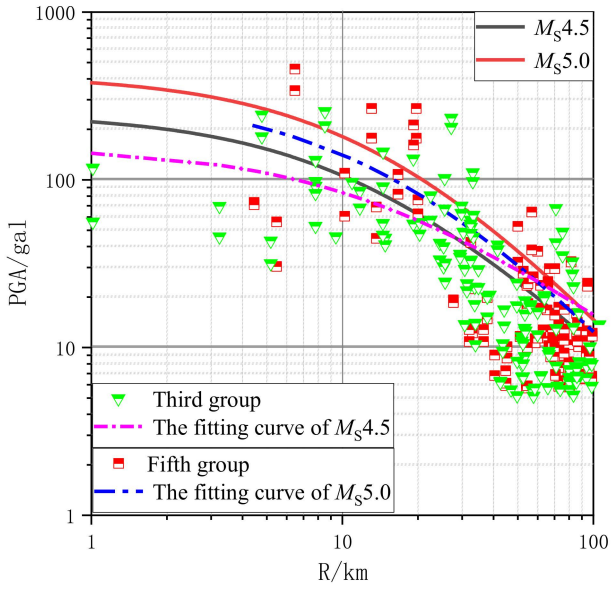


Figure 13. Comparison of PGA attenuation curves and PGA observed values.

5. Model Regression Results

Regression analyses are conducted using magnitude grouping methods with Models I and II to predict the equations for horizontal PGA, EPA, and PGV, utilizing the ground motion attenuation dataset for the Loess Plateau region. The corresponding results are listed in Table 5, which reports the prediction equations for Models I and II and their corresponding standard deviations, i.e., the standard deviation of the fitting residuals. Model II demonstrates better fitting performance than Model I, indicated by lower residuals. For instance, the standard deviation for the PGA prediction equation established by Model I is 0.457 while it is 0.342 for Model II.

Table 5. Horizontal ground motion peak prediction equations for the Loess Plateau region.

Parameter	Prediction Equation	Model	Standard Deviation
PGA	$\lg PGA = 4.916 + 0.867M - 4.085\lg\left(R + 9.669e^{0.303M}\right)$	I	0.457
	$\lg PGA = -1.399 + 1.186M + (0.468 - 0.422M)\lg\left(R + 2.290e^{0.373M}\right)$	II	0.342
EPA	$\lg EPA = 4.797 + 0.873M - 4.119\lg\left(R + 9.217e^{0.303M}\right)$	I	0.493
	$\lg EPA = -2.443 + 1.476M + (0.921 - 0.554M)\lg\left(R + 3.650e^{0.350M}\right)$	II	0.357
PGV	$\lg PGV = 3.451 + 0.573M - 3.152\lg\left(R + 20.0e^{0.141M}\right)$	I	0.345
	$\lg PGV = -3.123 + 1.693M + (0.654 - 0.642M)\lg\left(R + 20.0e^{0.148M}\right)$	II	0.329

5.1. PGA Attenuation Relationship

Figure 14 compares the horizontal PGA attenuation curves for different magnitudes, with solid lines representing the attenuation curves based on Model I and dashed lines (including dot-dashed lines and other line types) representing the attenuation curves based on Model II. Figure 14 infers that when the magnitude is $M_S \leq 5.0$, the attenuation rate of Model I is noticeably faster than that of Model II.

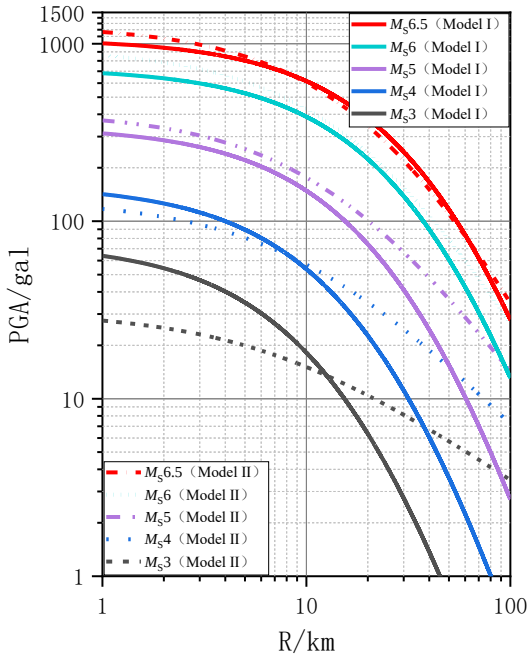


Figure 14. Comparison of PGA attenuation curves between Model I and Model II.

The ground motion parameters derived from strong motion record data analysis, such as PGA, are called "observed values". Meanwhile, those calculated through ground motion parameter prediction equations are termed "predicted values". Figure 15 selects two sets of observed values with average magnitudes of M_S 4.2 and M_S 5.0 for comparison against the attenuation curves. Figure 15 reveals few observed values at epicentral distances R < 10 km, especially within R < 4 km, indicating a lack of sufficient samples near the epicenter to effectively control the epicentral fitting accuracy of the prediction equations. In regions with epicentral distances R > 50 km, the observed values for average magnitudes of M_S 5.0 and M_S 4.2 mix, indicating a high dispersion in PGA observed values, which do not increase significantly with increasing magnitude.

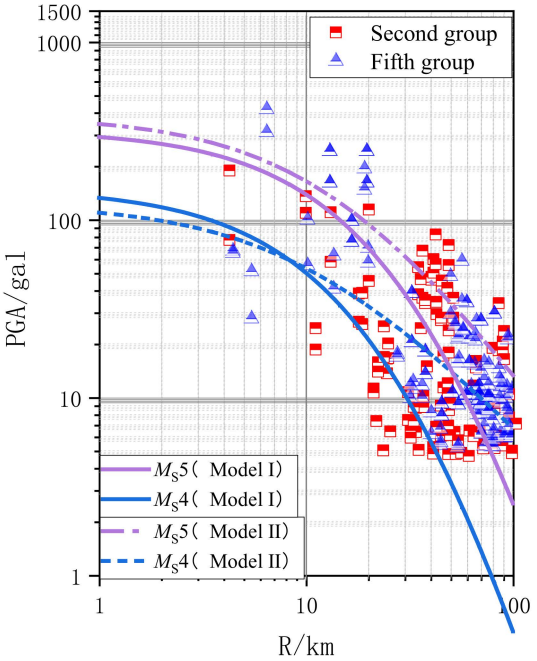


Figure 15. Comparison of PGA prediction curves with observed values.

5.2. EPA Attenuation Relationship

The attenuation curves for the EPA prediction equations are depicted in Figure 16, with the attenuation characteristics of Models I and II broadly consistent with those of PGA. In the region with epicentral distances $R < 10$ km, for earthquakes of magnitudes M_S 3.0 and M_S 4.0, the horizontal EPA attenuation curves from Model I are higher than the predicted values from Model II. However, as the epicentral distance increases beyond $R > 10$ km, the predicted values from Model I gradually reduce due to its faster attenuation rate. For magnitudes $M_S > 5.0$, the horizontal EPA attenuation curves from Model II are slightly higher than those from Model I. At M_S 6.5, the attenuation curves from both models nearly coincide. Figure 17 compares the EPA observed values and attenuation curves, illustrating that the fit in Model II is superior to Model I.

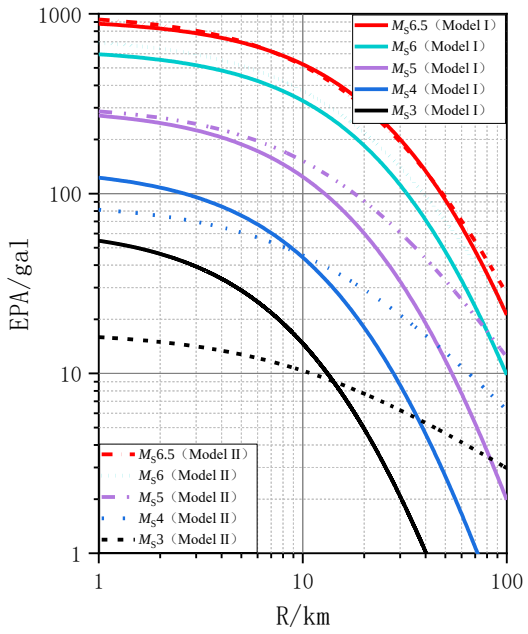


Figure 16. Comparison of EPA attenuation curves between Model I and Model II.

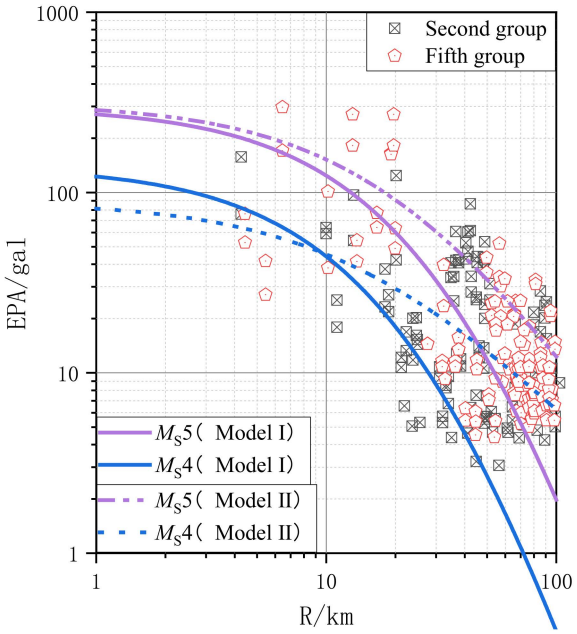


Figure 17. Comparison of EPA prediction curves with observed values.

5.3. PGV Attenuation Relationship

Figure 18 compares the horizontal PGV attenuation curves for different magnitudes. Near the epicenter (R = 1 km), the PGV predictions for Model I and Model II are as follows: for a M_S 6.5 earthquake, 63 cm/s and 64 cm/s, respectively; for a M_S 6.0 earthquake, 40 cm/s and 41 cm/s; for a M_S 5.0 earthquake, 17 cm/s and 15 cm/s; for a M_S 4.0 earthquake, 7 cm/s and 4 cm/s; and for a M_S 3.0 earthquake, 3 cm/s and 1 cm/s. Near the epicenter, when the magnitude exceeds M_S 5.0, the PGV predictions of the two models are similar while, for magnitudes less than M_S 5.0, Model I's predictions are higher than those of Model II. Figure 19 compares the PGV observed values and attenuation curves, indicating that the fit of Model II is superior to that of Model I.

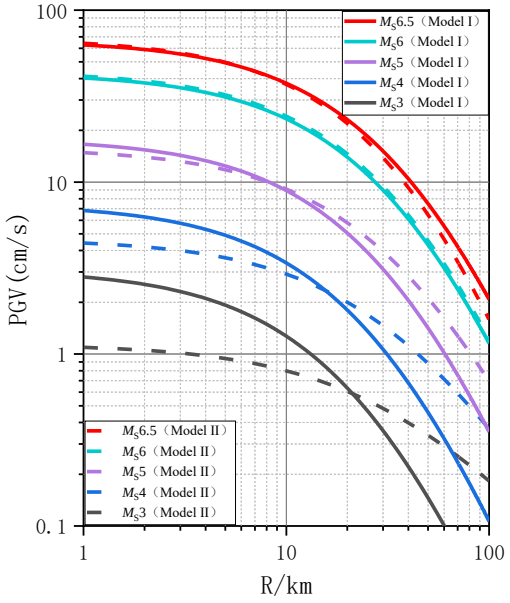


Figure 18. Comparison of PGV attenuation curves between Model I and Model II.

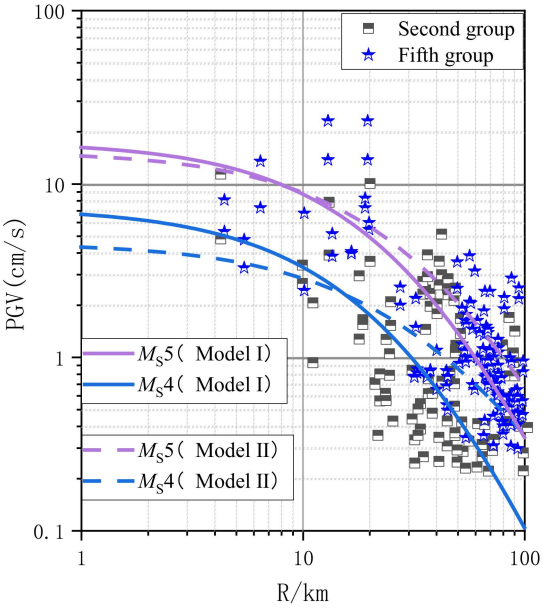


Figure 19. Comparison of PGV prediction curves with observed values.

6. Residual Analysis of Horizontal Peak Parameter Attenuation Relationships

In this section, the residuals refer to the logarithmic differences (Base 10) between the observed and predicted values from the strong motion records, which are the logarithms of the observed values minus the logarithms of the predicted values. The observed values are from the attenuation research dataset while the predicted values are calculated based on the peak prediction equations presented in this paper. Figure 20 depicts the distribution of PGA fitting residuals based on epicentral distance and Figure 21 illustrates the distribution of PGA fitting residuals based on magnitude.

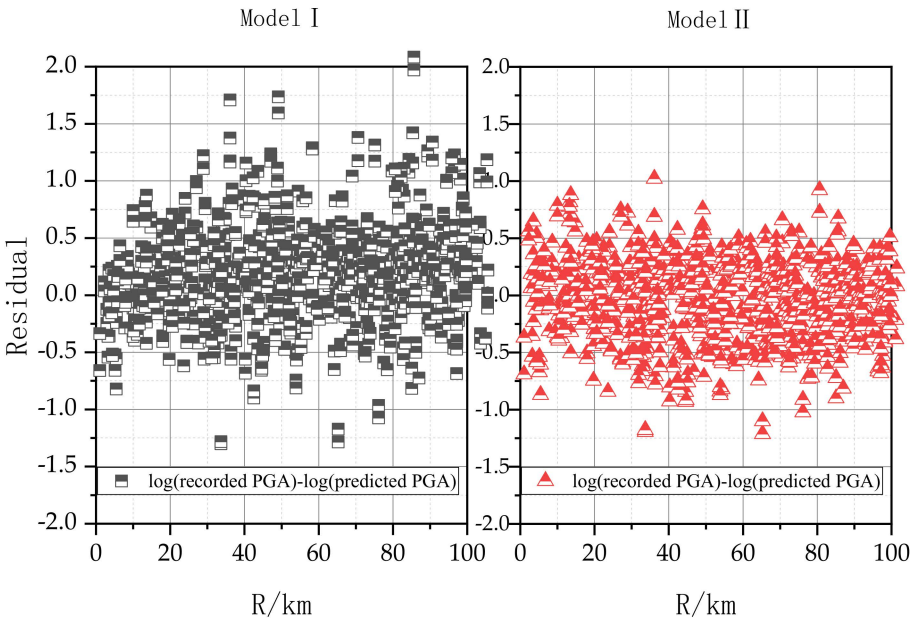


Figure 20. Distribution of PGA fitting residuals by epicentral distance.

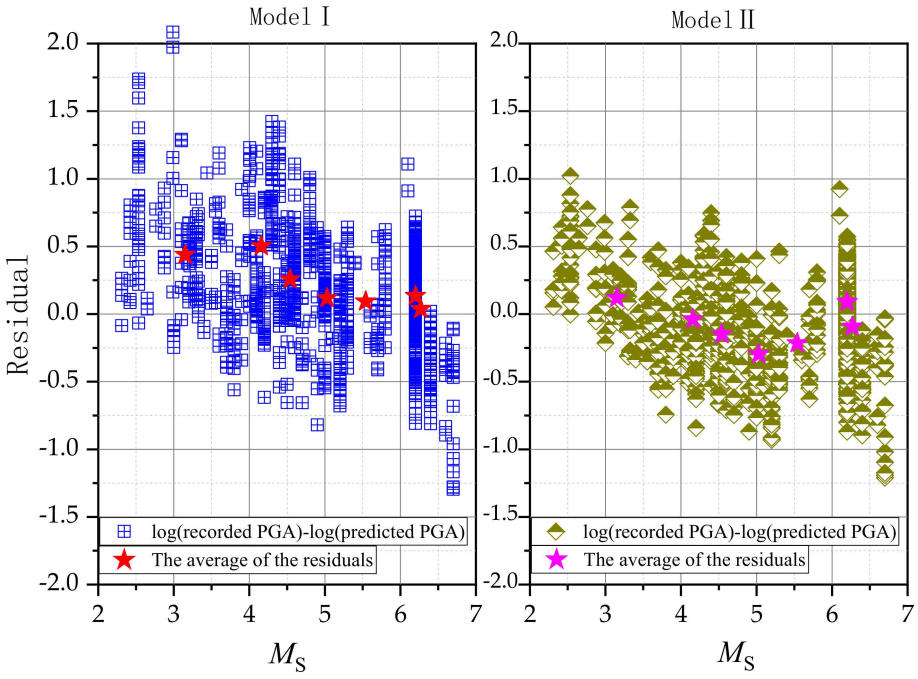


Figure 21. Distribution of PGA fitting residuals by magnitude.

The left chart in Figure 20 displays the distribution of PGA residuals for Model I, for a residual range of −1.30 to 2.08 and an average of all residuals of 0.196. The right chart displays the PGA residuals for Model II, with a residual range of −1.21 to 1.02 and an average of all residuals of −0.0657. Comparing the two charts reveals that the fitting residuals for Model II are smaller than those for Model I, indicating that Model II provides a better fit than Model I.

In Figure 21, the left and right charts represent the distribution of residuals for Model I and Model II, with pentagrams marking the arithmetic mean of residuals for different magnitude brackets. For Model I, the average residuals for each magnitude bracket are as follows: M_S 3.2 at 0.44, M_S 4.2 at 0.50, M_S 4.5 at 0.26, M_S 5.0 at 0.12, M_S 5.5 at 0.09, M_S 6.2 at 0.13, and M_S 6.3 at 0.04. For Model II, the corresponding values are M_S 3.2 at 0.12, M_S 4.2 at −0.04, M_S 4.5 at -0.15, M_S 5.0 at −0.30, M_S 5.5 at −0.22, M_S 6.2 at 0.09, and M_S 6.3 at −0.09.

Hence, there are differences in Model I and Model II performance under various magnitude conditions. Model I underestimates the PGA values for magnitudes less than M_S 4.5 and Model II slightly overestimates the PGA values for magnitudes between M_S 4.5 and M_S 5.5. For magnitudes less than M_S 4.5, the predictions from Model II are more accurate, whereas, for magnitudes between M_S 4.5 and M_S 5.5, the predictions from Model I are more favorable. When the magnitude exceeds M_S 5.5, the prediction accuracy of the two models is comparable.

Figure 22 displays the distribution of fitting residuals for EPA, where the left chart refers to Model I, ranging from −1.28 to 2.17 with an average of 0.23, and the right chart refers to Model II, ranging from −1.24 to 1.09 with an average of -0.08. Comparing the two charts indicates that Model II has smaller residuals and a superior fitting result than Model I.

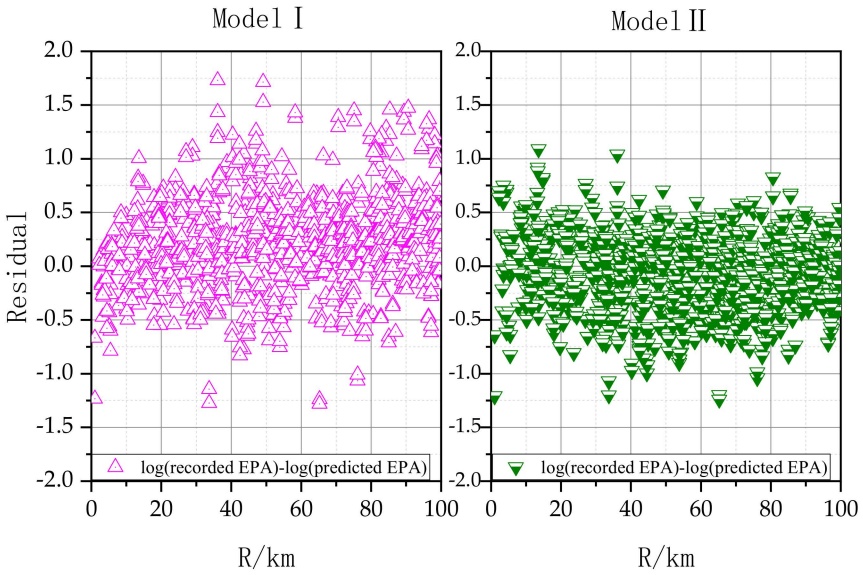


Figure 22. Distribution of EPA fitting residuals by epicentral distance.

Figure 23 presents the EPA residuals for different magnitude brackets, where the left chart refers to Model I and the right for Model II, with pentagrams indicating the arithmetic mean of residuals for each magnitude. The trend in the distribution of the EPA residuals is roughly consistent with that of PGA. The average residuals for Model I are M_S 3.2 at 0.46, M_S 4.2 at 0.57, M_S 4.5 at 0.32, M_S 5.0 at 0.20, M_S 5.5 at 0.15, M_S 6.2 at 0.10, and M_S 6.3 at 0.06; for Model II, they are M_S 3.2 at 0.15, M_S 4.2 at −0.03, M_S 4.5 at −0.14, M_S 5.0 at −0.28, M_S 5.5 at −0.22, M_S 6.2 at 0.01, and M_S 6.3 at −0.12. Thus, Model I tends to overpredict at lower

magnitudes while Model II's predictions are more accurate, particularly for magnitudes below M_S 4.5.

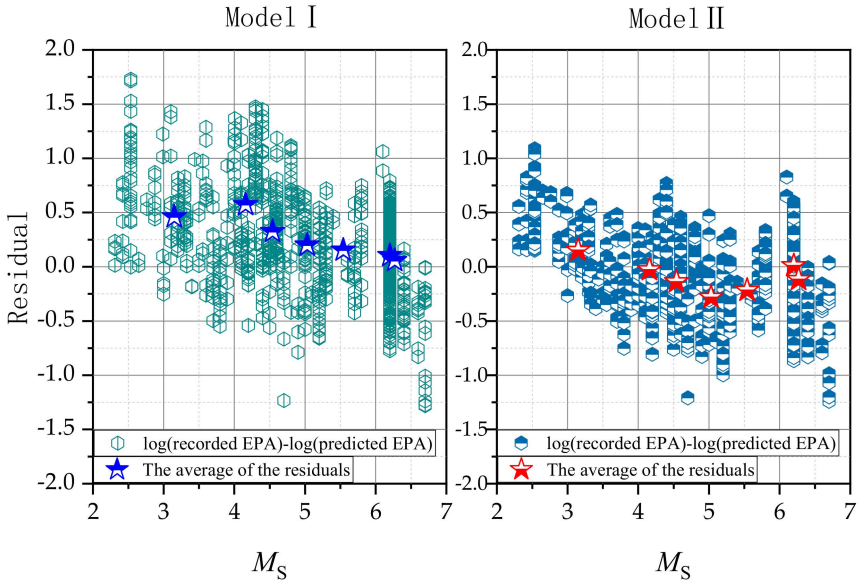


Figure 23. Distribution of EPA fitting residuals by magnitude.

Figure 24 illustrates the distribution of fitting residuals for PGV based on epicentral distance. The left chart displays the PGV residual distribution for Model I, ranging from −1.41 to 1.27, with an average value of −0.01, and the right diagram shows the PGV residual distribution for Model II, ranging from −1.28 to 1.00, with an average value of −0.08. The distributions reveal that Model II's fitting residuals are slightly lower than those of Model I, indicating that Model II's PGV fitting performance is marginally better than Model I's. Overall, whether for PGA, EPA, or PGV, Model II's predictive performance exceeds that of Model I, especially under conditions of low magnitude and large epicentral distance.

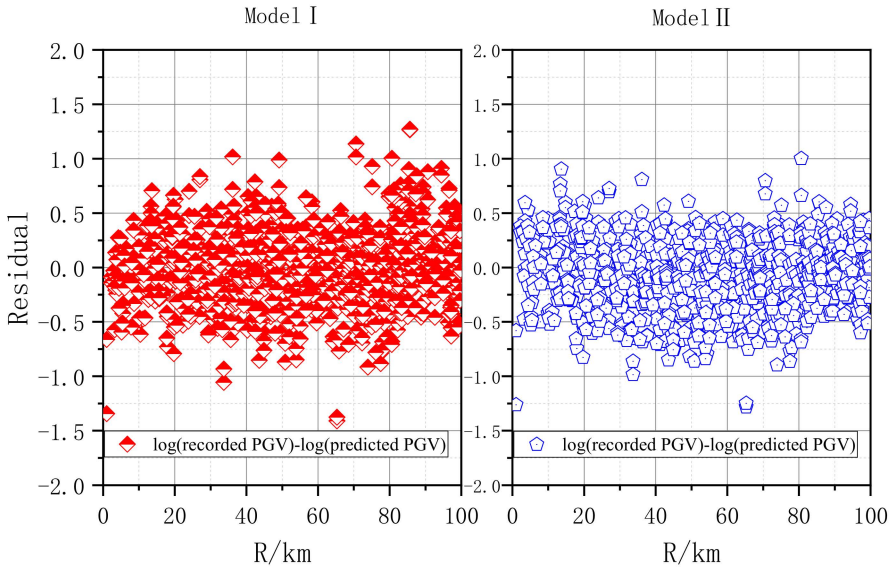


Figure 24. Distribution of PGV fitting residuals by epicentral distance.

Figure 25 displays the distribution of PGV fitting residuals based on magnitude. The chart reveals that the range of PGV residuals varies across different magnitudes and the average residual values differ per magnitude bracket. For Model I, the average residuals are M_S 3.2 at 0.10, M_S 4.2 at 0.19, M_S 4.5 at 0.06, M_S 5.0 at 0.01, M_S 5.5 at −0.04, M_S 6.2 at

−0.09, and M_S 6.3 at −0.12. For Model II, the corresponding average residuals are M_S 3.2 at 0.05, M_S 4.2 at −0.05, M_S 4.5 at −0.12, M_S 5.0 at −0.17, M_S 5.5 at −0.16, M_S 6.2 at 0.09, and M_S 6.3 at −0.09.

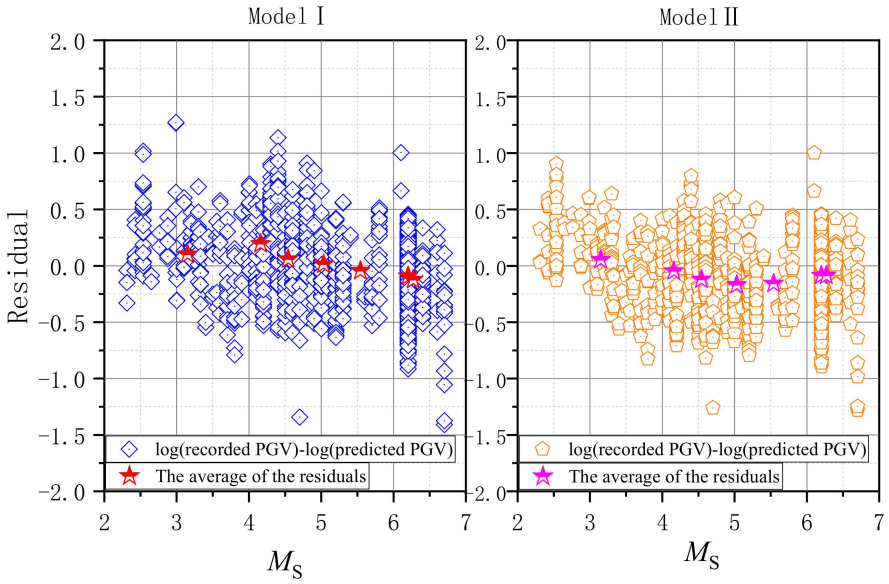


Figure 25. Distribution of PGV fitting residuals by magnitude.

Overall, PGV fitting residuals are slightly smaller compared to PGA and EPA. For magnitudes less than M_S 5.0, Model I's PGV predictions are somewhat lower than the observed values. For magnitudes greater than M_S 5.0, Model I's predictions are slightly overestimated. Additionally, within the magnitude range of M_S 4.0 to M_S 6.5, Model II's PGV predictions tend to slightly overestimate compared to the observed values. This suggests that different models have varying predictive accuracies across different magnitude ranges, necessitating the selection of appropriate models based on specific magnitude ranges to enhance prediction accuracy.

7. Conclusions

This paper introduces the attenuation research dataset for the Loess Plateau region, details the data processing methods, and analyzes the distribution of strong motion records. It also presents two attenuation relationship models and two-step fitting methods. The results indicate that the magnitude grouping scheme effectively reduces the dispersion of statistical samples in the magnitude component, thereby improving the fitting results. Based on regression statistics on 1149 data samples using the proposed models, Models I and II, we derive the prediction equations for PGA, EPA, and PGV for horizontal soil layers in the Loess Plateau region and plot the corresponding attenuation relationship graphs.

A comparative analysis between the observed values and the prediction equation curves provides the following conclusions:

(1) For magnitudes $\geq M_S$ 6.0, the fitting results of attenuation Models I and II are quite close. However, for magnitudes less than M_S 6.0, the differences gradually increase as the magnitude decreases;

(2) Model I uses a fixed attenuation coefficient, which does not vary with magnitude, resulting in parallel attenuation curves. In contrast, Model II's attenuation coefficient is a linear function of magnitude, leading to a faster attenuation rate as magnitude increases, causing the different magnitude attenuation curves of Model II to converge at greater epicentral distances;

(3) By comparing the observed values and prediction equation curves for magnitudes M_S 4.2 and M_S 5.0, it is apparent that Model II slightly outperforms Model I, exhibiting a lower standard error in fitting ground motion parameters;
(4) When comparing the standard deviations, Model II's fitting results are slightly better than those of Model I, with its fitting standard deviation about 80% of that of Model I. Analyzing the residual distribution for peak parameter attenuation reveals differences in the average residuals across magnitude brackets, with most brackets showing lower overall deviations using Model II. However, some brackets still show smaller fitting deviations with Model I. Considering the advantages and disadvantages of both models, this paper uses both attenuation models to establish ground motion parameter prediction equations for the Loess Plateau region;
(5) When using the seismic motion parameter prediction equations provided in this paper, to ensure safety, it is recommended to calculate the predictions of both Model I and Model II and use the higher of the two values as the basis for seismic design calculations.

Author Contributions: Conceptualization, J.B. and W.W.; methodology, W.W.; software, D.P.; validation, W.W.; formal analysis, W.W.; investigation, W.W.; data curation, W.W. and D.P.; writing—original draft preparation, W.W.; writing—review and editing, J.B. and D.P.; visualization, W.W.; supervision, J.B.; project administration, W.W. All authors have read and agreed to the published version of the manuscript.

Funding: This work was funded by the Hebei Key Laboratory of Earthquake Disaster Prevention and Risk Assessment (No. FZ201101), the Science Research Project of Hebei Education Department (No. QN2021308), and the Fundamental Research Funds for the Central Universities (No. ZY20215128).

Institutional Review Board Statement: Not applicable.

Informed Consent Statement: Not applicable.

Data Availability Statement: The strong motion data used in this study were obtained from the Strong Motion Observation Center of the Institute of Engineering Mechanics, China Earthquake Administration.

Acknowledgments: The authors extend their sincere gratitude to the Strong Motion Observation Center of the Institute of Engineering Mechanics, China Earthquake Administration, for providing invaluable strong motion data from the Loess Plateau region of China. Special thanks are also due to the China Earthquake Networks Center for supplying extensive strong motion data that served as a crucial foundation for this study. Additionally, the authors acknowledge EditSprings (https://www.editsprings.cn) for their professional linguistic support.

Conflicts of Interest: The authors declare no conflicts of interest.

References

1. Wang, L.; Sun, J. Seismic Safety Issues in Urban Construction on the Loess Plateau. *Earthq. Eng. Eng. Dyn.* **2014**, *34*, 115–122. (In Chinese)
2. Bo, J.; Wan, W.; Peng, D.; Duan, Y.; Li, Q. Advances in Ground Motion Attenuation Relationship Research in the Loess Plateau of China. *J. Earthq. Eng.* **2024**, *46*, 182–198. (In Chinese)
3. Hu, Y.; Zhang, M. Methods for Estimating Ground Motion Parameters in Areas Lacking Strong-Motion Records. *Earthq. Eng. Eng. Dyn.* **1984**, *4*, 1–11. (In Chinese)
4. Hu, Y.; Zhou, K.; Yan, X. Mapping Methods for Ground Motion Estimation in Areas without Acceleration Records. *Earthq. Eng. Eng. Dyn.* **1996**, *16*, 1–10. (In Chinese)
5. Ding, B.; Lei, Z.; Fang, S. Empirical Attenuation Relationships of Bedrock Ground Motion in the Loess Region of China. *Northwestern Seismol. J.* **1988**, *10*, 57–65. (In Chinese)
6. Wen, C. Analysis and Determination of Ground Motion Attenuation Relationships in Shanxi. *North China Earthq. Sci.* **1991**, *9*, 74–81. (In Chinese)

7. Zhou, Z.; He, S.; Chen, W. Study on Seismic Intensity Attenuation Relationships in Gansu Province. *J. Earthq. Eng.* **2010**, *32*, 72–75. (In Chinese)
8. Fan, W.; Du, W.; Wang, X.; Shao, H.; Wen, Y. Research on Ground Motion Attenuation Relationships in Shaanxi Region. *Earthq. Eng. Eng. Dyn.* **2011**, *31*, 47–54. (In Chinese)
9. Yang, F.; Luo, Q.; Li, B.; Che, W. Peak Ground Acceleration Attenuation Relationships for Loess Regions in China Based on the Wenchuan Earthquake. *J. Beijing Univ. Technol.* **2011**, *37*, 1487–1492. (In Chinese)
10. Xiao, L.; Yu, Y. Seismic Intensity Attenuation Relationships in Western China. *Technol. Earthq. Disaster Prev.* **2011**, *6*, 358–371. (In Chinese)
11. Yang, Y.M.; Dai, Y.; Zhang, G.; Wang, L.; Zhao, X.; Wang, J.M. Seismic Intensity Attenuation Relationships for the Central and Western Regions of Inner Mongolia. *Earthq. Geomagn. Obs. Res.* **2016**, *37*, 30–37. (In Chinese)
12. Yang, W.; Wang, C.; Xu, W.; Du, K.; Yu, D. Seismic Intensity Attenuation Relationships in the North-South Seismic Belt. *World Earthq. Eng.* **2021**, *37*, 207–218. (In Chinese)
13. Yuan, Y.; Tian, Q. *Engineering Seismology*; China Earthquake Press: Beijing, China, 2012; pp. 91–105. (In Chinese)
14. Iwan, W.D.; Moser, M.A.; Peng, C. Strong-motion earthquake measurement using a digital accelerograph. *Bull. Seismol. Soc. Am.* **1985**, *75*, 1225–1246. [CrossRef]
15. Yu, Y. Seismic Ground Motion Estimation Models in the Wenchuan Earthquake Area. Ph.D. Thesis, Institute of Engineering Mechanics, China Earthquake Administration, Beijing, China, 2012. (In Chinese)
16. China Earthquake Disaster Prevention Center. *Earthquake Work Handbook*; China Earthquake Disaster Prevention Center: Beijing, China, 1990.
17. GAO M. *The Textbook GB 18306-2015 Zoning Map of Ground Motion Parameters in China Was Publicized*; China Quality Inspection Press: Beijing, China, 2015; pp. 175–180.
18. Chen, D.; Liu, H. Elliptical Attenuation Relationship of Seismic Intensity. *North China Earthq. Sci.* **1989**, *7*, 31–42. (In Chinese)
19. Sha, H.; Lü, Y.; Peng, Y.; Tang, R.; Zhang, X. A Constrained Model of Elliptical Attenuation of Seismic Intensity and Its Application in North China. *J. Disaster Prev. Mitig. Eng.* **2004**, *24*, 28–36. (In Chinese)
20. Joyner, W.B.; Boore, D.M. Peak horizontal acceleration and velocity from strong-motion records from the 1979 Imperial Valley, California, earthquake. *Bull. Seismol. Soc. Am.* **1981**, *7*, 2011–2038. [CrossRef]
21. Wang, G.; Tao, X. A New Two-Step Method for Fitting Seismic Attenuation Relationships. *Earthq. Eng. Eng. Vib.* **2001**, *21*, 24–28. (In Chinese)

Disclaimer/Publisher's Note: The statements, opinions and data contained in all publications are solely those of the individual author(s) and contributor(s) and not of MDPI and/or the editor(s). MDPI and/or the editor(s) disclaim responsibility for any injury to people or property resulting from any ideas, methods, instructions or products referred to in the content.